P4.12 Diagnosed Structure of the Mulhall Tornado Using VTD Algorithm

Wen-Chau Lee[#] Joshua Wurman[*]
[#]National Center for Atmospheric Research[1], Boulder CO, 80307
[*]University of Oklahoma, Norman, OK, 73019

1. Introduction

Tornadoes are among one of the most violent storms in the world. Because of their small temporal and spatial scale, mapping of tornado winds have mostly eluded Doppler radar (e.g., WSR-88D) observations until the mobile 3-cm Doppler on Wheels (DOW, Wurman et al. 1997; Wurman 2001) and the 3-mm Dopper radar (Bluestein and Pazmany 2000) was placed in service in 1995. DOWs can be deployed as close as 150 m from a tornado to sample high-resolution single- and dual-Doppler radar measurements (e.g., Wurman and Gill 2000). Some tornado structures, such as maximum wind and peak vorticity, can be inferred from single Doppler radar mesocyclone signatures (e.g., Wurman 2002). The purpose of this paper is to diagnose the axisymmetric and asymmetric vortex structures of the Mulhall tornado from data collected by a single DOW and the ground-based velocity track display (GBVTD, Lee et al. 1999) technique. Kinematic and dynamic characteristics of this tornado are compared with laboratory and numerically simulated tornados.

2. Storm overview and data processing

On 3 May 1999, a supercell thunderstorm with a pronounced hook echo and an intense cyclonic circulation was identified by the Norman, OK WSR-88D radar. This thunderstorm, observed by the DOW from 0310-0328 UTC, produced an exceptionally large and powerful tornado with ~800 m in peak wind radius and peak wind speeds exceeding 100 m/s. The evolution of the reflectivity structures and multiple vortices embedded in the parent tornado circulation were documented in Wurman (2002). Scanning was conducted through ~85° azimuthal sectors at 12 stepped elevation angles from 0-17°. Each volume scan took about 1 minute to complete. The core region of the tornado moved to a range of ~3.5-4.5 km from DOW, resulting in a radar beam width of 65 m, and 25-37.5 m gate spacing. Staggered pulse repetition frequency resulted in a Nyquist velocity of ±128 m/s. The data were edited using the NCAR SOLO software. The radar beams were partially blocked by terrain and trees below approximately 1.5° elevation angle at various azimuth angles resulting in possible contamination of the measurements. The return power is used in this paper because the reflectivity factor cannot be reliably computed due to problems in calibration and receiver saturation from large debris and rain field of the tornado at close range (Wurman 2002).

The GBVTD analysis was performed with a 100 m increment in radius, r, (200 m < r < 3 km) and altitude, z, (100 m < z < 1.2 km) axes. The vorticity centers of the parent tornado circulation at each altitude were objectively determined using the GBVTD-simplex algorithm (Lee and Marks 2000; Bell and Lee 2002). Then, the asymmetric tornado circulation was deduced up to wavenumber 10. The highest wavenumber in the GBVTD analysis is determined by the maximum data gap in the Doppler velocity data along a constant radius that is required to stabilize the least-squares curve fit. The objective center finding method took into account the spatial and time continuity of the maximum mean tangential wind, the radius of maximum wind (RMW) and the x and y position of the tornado vorticity center.

The axisymmetric angular momentum, vorticity, perturbation pressure and swirl ratio were computed using the GBVTD-derived axisymmetric tangential (v) and radial (u) winds. The radial pressure equation in cylindrical coordinates is:

$$\rho\left(\underbrace{u\frac{\partial u}{\partial r}+w\frac{\partial u}{\partial z}}_{Advection}\ \underbrace{-\frac{v^2}{r}}_{Cyclostrophic}\right)=-\frac{\partial p}{\partial r} \qquad (1)$$

where ρ is the density while *p* is the perturbation pressure obtained by integrating the pressure gradient from the outer domain at r=3 km at each altitude.

3. Structure of the Mulhall Tornado

Figure 1 illustrates the axisymmetric structure of the tornado at 0310 UTC, 4 May 1999. The gray scale represents the return power. The axisymmetric *v* (Fig. 1a) shows a maximum exceeding 70 m/s at r=900 m and z=100 m. *v* decreases and tilts outward slightly with height. The radial flow, u, shows a deep layer inflow (~1 km) converging with the outflow from the tornado center at r=~900 m, the RMW (Fig. 1b). The peak inflow at z=100 m exceeds 20 m/s while the peak outflow of 12 m/s inside RMW is located at r=500 m and z=200 m. The axisymmetric vertical velocity, *w*, is obtained by vertically integrating the mass continuity equation upward using the axisymmetric convergence field computed from *u*. It is evident that it is a "two-celled" structure (e.g., Rotunno 1978; Ward 1972) with an intense downdraft (~25 m/s) at r=300 m and z=900 m. Although Wurman and Gill (2000) observed evidence of a downdraft with similar magnitude in the Dimmitt tornado, this is the first time that a downdraft inside the tornado core is retrieved from single Doppler radar data.

[1] Corresponding author address: Dr. Wen-Chau Lee, NCAR Remote Sensing Facility, Boulder, CO 80307. NCAR is sponsored by the National Science Foundation.

This "two-celled" structure persisted for the next 14 volumes. The depth of the inflow is ~600 m except for the first volumes (Table 1). Because considerable debris was likely lofted by the tornado, it is possible that DOW is measuring the debris motion instead of the air motion. Debris and large raindrops would likely be thrown out of the tornado circulation due to centrifugal force and the convergence field may be biased (Wurman and Gill 2000; Dowell et al. 2001). Estimates of centrifuging effects in this storm indicate that the bias to the radial winds is ~4 m/s near the RMW. As a result, the zero Doppler velocity line of the air motion should probably be ~100 m closer to the tornado center from the measured location in Fig. 1. Nevertheless, the generality of the results presented in this study will not be affected.

Figures 1c and 1d illustrate the retrieved perturbation pressure from the advection and cyclostrophic terms in (1), respectively. The cyclostrophic pressure is in response to the swirling part of the tornado circulation while the pressure from advection terms is in response to the secondary circulation. The central cyclostrophic pressure (Fig. 1d) at z=100 m is ~75 mb lower than the pressure at r=3 km. The total pressure drop is consistent with observed pressure drop in a similar storm (Winn et al. 1999). The pressure from advection terms is an order of magnitude smaller than the pressure from cyclostrophic balance. The low-level pressure perturbation gradient is consistent with the radial wind pattern, such as outflow from the center, inflow from the environment and the slow down of *u* near the convergence zone.

Figure 1e and 1f illustrate the angular momentum and vorticity of this tornado. The angular momentum increases with radius. Hence, the low-level inflow brings in higher angular momentum. The peak vorticity of 0.2 s^{-1} is located slightly inside the peak tangential winds. The vorticity has a ring profile at this time which is also a necessary condition for existence of barotropic instability. Near zero but negative vorticity is located outside RMW below 600 m altitude. The flow beyond r=1.2 km is near potential flow.

The evolution of the Mulhall tornado can be shown in Hovmoller diagrams at z=100 m (Fig. 2). The axisymmetric tangential winds (top panel) show a decreasing RMW from ~800 m to ~500 m from 131003 to 131513 while the maximum tangential winds decrease with time. Then the RMW increases slightly with time. The peak tangential wind occurs at 134628 exceeding 80 m/s. The intensification of the tangential wind is preceded by a pulse of radial inflow (> 15 m/s) at 131513 (middle panel). Note that the wind fields are obtained independently of each other. Therefore, the consistent features in time in Fig. 2 are very encouraging and lend confidence on the GBVTD-retrieved axisymmetric structures.

Consistent with the tangential wind pattern, the radial winds (middle panel) also show periods of enhanced inflow. The inflow collides with outflow at r~500 m before 131722. Then the convergence zone moves outward in radius from r~500 m to r~2500 m in the next 6 minutes. This suggests expansion of the updraft radius with time (not shown). The vorticity plot (bottom panel) illustrates that high vorticity is concentrated near or inside the RMW. The ring vorticity structure is accompanied by relatively strong axisymmetric tangential winds before 131722. After 131722, the vorticity shows a monopole profile signaling weakening of the tornado.

Another noteworthy feature of the Mulhall tornado is the evolution of the axisymmetric w. The Hovmoller diagram of axisymmetric w at z=700 m is shown in Fig. 3. Before 131259, the primary updraft is centered at the RMW with weak downdraft outside r=1.5 km. An outer updraft forms beyond r=1.5 km at 131416 and intensifies with time. The outer updraft becomes the primary updraft after 132110. Since the primary convergence zone also moves outward in radius, consistent with the intensification of the outer updraft, this feature is similar to the eyewall replacement process in an intense tropical cyclone (Willoughby et al. 1982). The peak downdraft intensity inside the tornado core remains strong (> 30 m/s) at z=700 m throughout the analysis period. It is also evident that the intensity of the downdraft decreases and the width increases as the outer updraft becomes the primary updraft.

4. The swirl ratio and multiple vortices

The Mulhall tornado possessed multiple vortices (Wurman 2002) that are clearly indicated by small reflectivity loops with corresponding Doppler velocity dipole structure (not shown). The formation of multiple vortices in the laboratory and numerical simulations of tornados strongly depends on a dynamical parameter, the swirl ratio. The swirl ratio (S) is defined as:

$$S = \frac{1}{4} c \tan\theta = \frac{1}{4} \cdot \frac{2R}{h} \cdot \frac{v_R}{u_R} \qquad \textbf{(2)}$$

where R, h, u_R, and v_R are the updraft radius, inflow depth, radial and tangential winds at R, the radius of the outer bound of the tornado axisymmetric updraft (Rotunno 1978). The swirl ratio of the tornado can be computed in (2) using the GBVTD-derived axisymmetric circulation (Table 1). Both the laboratory and numerical simulations of tornado vortex suggest that a "one-celled" vortex transits into a "two-celled" vortex at S=0.5 while multiple vortices appear when S>1.0 (e.g., Davis-Jones 1973; Rotunno 1978). Because the swirl ratio was first defined in the parameters of the tornado vortex chamber (Davies-Jones, 1973), uncertainties in choosing the value of each term in real data (e.g., see Fig. 1a and 1b) may easily introduce a factor of 2 error in the computed swirl ratio. Nevertheless, this is the first attempt to compute swirl ratio in a real tornado scale using Doppler radar derived quantities. The swirl ratios in Table 1 are clearly greater than 1. The swirl ratio is consistent not only with the "two-celled" structure deduced by the GBVTD technique but also with the multiple vortices observed in this tornado (Wurman 2002).

The multiple vortices of the Mulhall tornado are apparent in the GBVTD-derived tangential winds (not shown). Although the least-squares fit is capable of

resolving up to wavenumber 10, meaningful amplitude can only be obtained up to wavenumber six which is not as high as shown in the reflectivity structure. The aliasing effect is primary due to the insufficient spatial resolution and temporal resolution of the DOW data to resolve vortices in 100 m scale or smaller. The asymmetric tangential wind structure will be shown during the conference.

5. Summary and future work

The data collected by DOW provided unprecedented temporal and spatial resolution on tornado events. The GBVTD technique, in conjunction with the DOW data, has allowed the retrieval of tornado circulations quantitatively from single Doppler radar data. This study illustrates the evolution and structures of the Mulhall tornado from the single DOW data and the GBVTD technique. The GBVTD-derived tornado circulation exhibits coherent temporal and spatial structures and characteristics consistent with laboratory and numerical simulated tornadoes. The Mulhall tornado reaches its peak intensity then decays during the observed period. The intensity oscillation in several minute scale and the decaying of the Mulhall tornado are captured in this dataset. Axisymmetric secondary circulations, vorticity, and perturbation pressures of the Mulhall tornado are also shown where they have not been deduced from single Doppler radar data in a tornado before.

With these new capabilities, It is now feasible to examine tornado dynamics using the GBVTD-derived wind fields, for example, the relationship between the barotropic instability and the formation of multiple vorticies. The possibility to apply the GBVTD technique on DOW in real-time is also an exciting possibility.

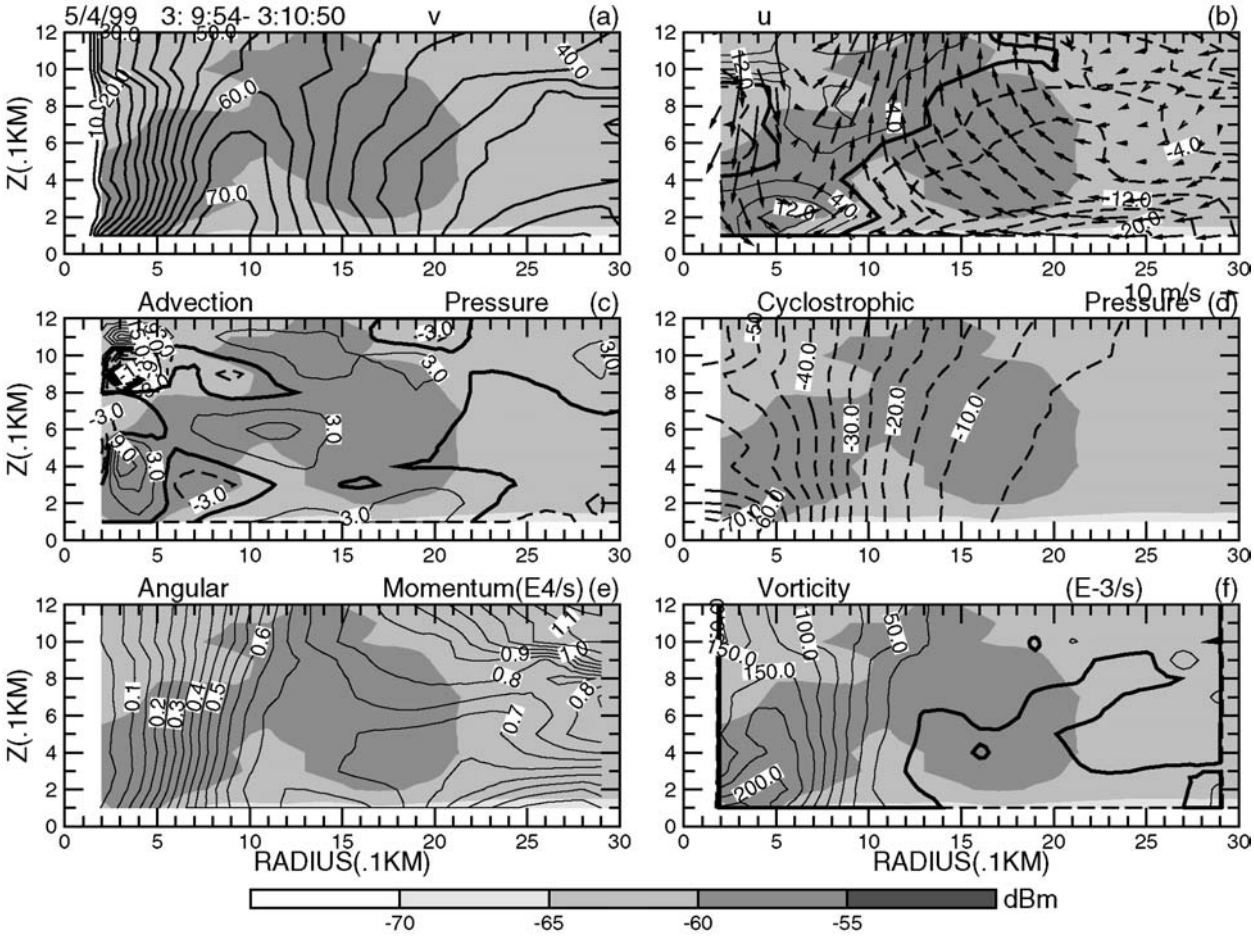

Figure 1: The axisymmetric circulation of the 5/4/1999 tornado at 0310 UTC where (a) tangential wind, (b) radial wind (contour) and velocity vector, (c) advection pressure, (d) cyclostrophic pressure, (e) unit mass angular momentum, and (f) vorticity. The return power is in gray shades.

Acknowledgment

The DOW program is a collaboration between University of Oklahoma and NCAR, supported by NSF and ONR. We thank Curtis

Alexander for assistance in processing DOW data. Mr. Michael Bell assisted in data editing, GBVTD analysis and generating figures.

References:

Bell, M, and W.-C. Lee, 2002: An objective method to select a consistent set of tropical cyclone circulation centers derived from the GBVTD-simplex algorithm. Preprints, 25th Conference on Hurricane and Tropical Meteorology. San Diego, CA., AMS, 642-643.

Bluestein, H. B., A. Z. Pazmany, 2000: Observations of tornadoes and other convective phenomena with a Mobile, 3-mm wavelength Doppler radar: The spring 1999 field experiment. *Bull. Amer. Metoror. Soc.,* **81**, 2939-2951.

Davies-Jones, R. P., 1973: The dependence of core radius on swirl ratio in a tornado simulator. *J. Atmos. Sci.,* **30,** 1427-1430.

Dowell, D. C., J. Wurman, and L. Wicher, 2001: Centrifuging of scatters in tornadoes. This volume.

Lee, W.-C., J.-D. Jou, P.-L. Chang, and S.-M. Deng, 1999: Tropical cyclone kinematic structure retrieved from single Doppler radar observations. Part I: Interpretation of Doppler velocity patterns and the GBVTD technique. *Mon. Wea. Rev*., **127,** 2419-2439.

Lee, W.-C., and F. D. Marks, 2000: Tropical cyclone kinematic structure retrieved from single Doppler radar observations. Part II: The GBVTD-simplex center finding algorithm. *Mon. Wea. Rev*., **128,** 1925-1936.

Rotunno, R., 1978: A study in tornado-like vortex dynamics. *J. Atmos. Sci.,* **36,** 140-155.

Ward, N. B., 1972: The exploration of certain features of tornado dynamics using a laboratory model. *J. Atmos. Sci.,* **29,** 1194-1204.

Winn, W. P., S. J., Hunyady, and G. D. Aulich, 1999: Pressure at the ground in a large tornado. *J. Geophy. Res.,* **104,** 22067-22082.

Wurman, J., 2001: The DOW mobile multiple Doppler network. Preprint, 30th International Conference on Radar Meteorology, Munich, Germany, AMS, 95-97.

Wurman, J., 2002: The multiple vortex structure of a tornado. Submitted to *Weather and Forecasting.* **17**, 473-505.

Wurman, J., and S. Gill, 2000: Finescale radar observations of the Dimmitt, Texas (2 June 1995), tornado. *Mon. Wea. Rev.,* **128,** 2135-2164.

Wurman, J., J. M. Straka, E. N. Rasmussen, M. Randall, and A Zahrai, 1997: Design and deployment of a portable, pencil-beam, pulsed, 3-cm Doppler radar. *J. Atmos. Oceanic Technol.,* **14,** 1502-1512.

UTC	*R (km)*	*H (km)*	u_R *(m/s)*	v_R *(m/s)*	*S*
131003	2.0	1.0	16	35	2
131057	1.5	0.5	16	40	3.8
131205	1.5	0.6	15	40	3.3
131259	1.5	0.5	10	40	6
131416	2.0	0.8	12	40	4.2
131513	2.5	0.6	16	30	3.9
131628	1.5	0.6	16	40	3.1
131722	1.5	0.6	8	32	5
131825	2.5	0.8	16	25	2.4
131918	2.8	0.7	20	20	2
132024	3.0	0.7	20	25	2.7
132120	3.0	1.0	18	25	2.1
132216	3.0	1.0	10	20	3.0
132312	3.0	1.0	12	20	2.5

Table 1: The swirl ratio (S) for 14 consecutive volumes of DOW data computed using equation (2).

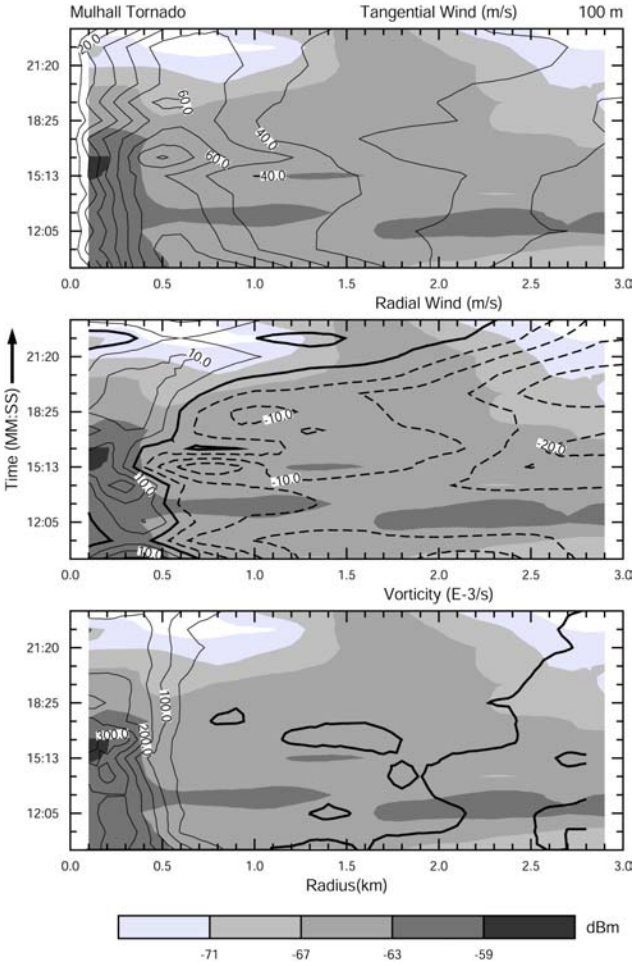

Figure 2: Hovmoller diagrams of axisymmetric return power (gray scale), tangential wind (top), radial wind (middle) and vorticity (lower) of the Mulhall tornado. Time increases from bottom to top. Thick, solid and dash lines represent zero, positive and negative values, respectively. Positive (negative) radial winds point away (toward) the tornado center.

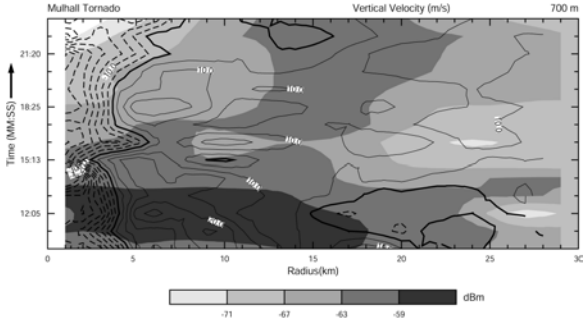

Figure 3: Hovmoller diagram of the axisymmetric return power (gray shades) and vertical velocities (contour) of the Mulhall tornado at z=700 m AGL. Solid (dash) lines represent updraft (downdraft) while the thick solid lines represent zero vertical velocity.